A molecular-dynamics study of medium-range order in molten trivalent metal chlorides

1994 J. Phys.: Condens. Matter 6 4405

(http://iopscience.iop.org/0953-8984/6/24/003)

J. Phys.: Condens. Matter 6 (1994) 4405–4418. Printed in the UK

A molecular-dynamics study of medium-range order in molten trivalent metal chlorides

Maria C Abramo and C Caccamo

Dipartimento di Fisica, Sezione Teorica, Università di Messina, CP 50, 98166 S Agata di Messina, Messina, Italy

Received 22 November 1993, in final form 14 February 1994

Abstract. Extensive molecular-dynamics (MD) simulations are performed for a rigid-ion model of molten metal trichlorides (MCl_3), in different regimes of metal radius, density and temperature. The cases of molten YCl_3 and $AlCl_3$ are examined in more detail in order to ascertain the presence of medium-range order (MRO) in these materials.

For the YCl_3 case, the experimental neutron structure factor, signalling the presence of MRO in the system, is fairly well reproduced by MD. The overall structural information available from the simulation indicates that order at intermediate distances basically consists of local 'layers' of corner-sharing $(YCl_6)^{3-}$ octahedra. These roughly planar formations may represent a remnant of the real YCl_3 crystalline structure, constituted by layers of edge-sharing $(YCl_6)^{3-}$ octahedra; the internal topology of the 'planes' is discussed in relation to the assumed model potential and to global charge ordering.

The effect of metal size on the MRO features is then investigated by adjusting the model parameters to the case of molten $AlCl_3$, in which the Al^{3+} effective radius is significantly smaller than that of Y^{3+}. In this case well defined tetrahedral $(AlCl_4)^-$ units tend to be formed, and these link to each other in a highly connected network responsible for MRO. The presence in the melt of bound pairs of tetrahedra, interpretable as Al_2Cl_3 'dimers', is also established, in essential agreement with the prediction of recent theoretical work by other authors.

1. Introduction

As is well known, the presence of a first sharp diffraction peak (FSDP) at small wavevectors in the (total) x-ray or neutron structure factor of many glasses and liquids (for a review on this argument, see [1]), like, for example, vitreous SiO_2, and molten and glassy chalcogenides, is considered as evidence of medium-range order (MRO) in those materials [1–3]. Recently, Saboungi *et al* [4] have reported the experimental neutron structure factor of molten YCl_3, showing a FSDP positioned at $k = 0.95$ Å^{-1}. On the basis of this result, and of other experimental data, the authors reconstruct the MRO of this fluid in terms of a network of $(YCl_6)^{3-}$ octahedra.

Recent papers by Tosi *et al* [5, 6], based on hypernetted chain (HNC) calculations for a charged soft-sphere model of molten trivalent metal chlorides (MCl_3) [7], have indicated that a key role is played by the metal and halogen relative ionic size, in determining both the local structure and the onset of MRO in these systems. An investigation of the MRO dependence on the sizes of the ionic components has also been recently performed for model molten chalcogenide compounds, and has led to similar conclusions [8].

In the molten MCl_3 case, in particular, the first anion coordination shell surrounding each metal is increasingly stabilized with the decreasing size of the latter; such a local property of the fluid results in the formation of well defined structural units able to connect to each other

0953-8984/94/244405+14$19.50

in a network arrangement, thus determining medium-range order [5, 6]. The characteristics of the network structure have been deduced in an indirect manner from experimental [4] and theoretical results [5, 6], while a direct reconstruction of the MRO topology, based on knowledge of angular correlations and statistics of the links between local structures, does not appear to be available yet.

In this paper we report the results of extensive molecular-dynamics (MD) simulations of molten MCl_3 salts. The simulations are all based on the same charged soft-sphere potential adopted in [5–7]. We first examine in detail the case of YCl_3 by comparing the MD structural results with experimental data and with previous HNC calculations [5, 6]; then, we reconstruct the medium-range structure of the system and try to ascertain whether and to what extent the layer structure proper of the real material in the crystalline phase is present in the liquid. The effects of density and temperature variations are also examined.

The properties of molten MCl_3 systems are then studied from a more general point of view, by examining how much the formation of local structural units and their arrangement at intermediate distances is affected by the metal size.

The cation radius is allowed to take values that may be appropriate to different real molten salts. In particular, major attention is devoted to the case of $AlCl_3$, since this substance is known to melt into a slightly ionized liquid of molecular Al_2Cl_6 dimers and the question arises [6] whether this type of molecule can be formed in a system governed by a simple rigid-ion potential, such as the one presently considered.

Finally, correlations between charge and medium-range order in the different metal radius regimes are also investigated.

It is worth observing that, given the simplified interaction law assumed, one cannot expect a quantitative agreement of MD results with structural experimental data. It is known, in fact, that the inclusion in the potential of three-body interaction terms and polarization effects [2, 3, 6, 9, 10] is a necessary prerequisite in order to obtain a faithful representation of the local structure of, for example, vitreous silica [9] and molten salts [10]. However, the importance of these same corrections in establishing and characterizing MRO does not seem unequivocally recognized [2, 3, 6, 9–11], and our study is also aimed at determining the role played in such a context by basic interaction mechanisms, like short-range repulsive and Coulombic forces. Obviously, a comparison of MD predictions for thermodynamic quantities, like internal energy and compressibility, with the corresponding experimental values would be desirable in this same concern. Unfortunately, the related data seem to be lacking.

The potential and the MD procedure are introduced in section 2. Section 3 reports structural results for molten YCl_3. The temperature and density effects on the MRO features, and an estimate of the ionic self-diffusion coefficients, are also reported here. Section 4 contains a broad analysis of the MD structural information as a function of the metal cation size. A short discussion and conclusions follow in section 5.

2. Model potential and simulation procedure

By following [5, 6], we assume that the potential consists of a soft spherical repulsive term at short range, and Coulombic interaction:

$$v_{ij}(r) = Z_i Z_j e^2/r + f(\rho_i + \rho_j)\exp[(R_i + R_j - r)/(\rho_i + \rho_j)]. \qquad (1)$$

Here Z_i, R_i and ρ_i are the valence, effective radius and effective hardness parameter in the ith ionic species, respectively. The value of f and the manner in which the other parameters are chosen will be specified in what follows.

Molecular-dynamics calculations were performed in the microcanonical ensemble with different particle numbers N and cubic box edge lengths L. In the case of molten YCl_3, $N = 664$ and L was fixed to reproduce the YCl_3 number density of particles at the neutron experiment temperature [4]. Most of the simulations, however, were performed with 340 particles, after having verified that the MD predictions practically do not change with respect to the 664-particles simulation, and that the simulation box edge length is in any case substantially greater than the MRO characteristic length scale ($\leqslant 6.5$ Å [4]). This is clearly visible in table 1 where box sizes, and other simulation parameters relative to the different metal radii, temperatures and densities investigated are reported.

A simulation time step $\tau = 0.2 \times 10^{-14}$ s and the Ewald summation method were employed. Unless otherwise specified, the system was started from a configuration in which the ionic particles are distributed at random on an FCC lattice, and then melted at the requested temperature with 4000 equilibration steps. Once a fully disordered liquid configuration was obtained, the system was left to run freely for a further 10000 time steps with averages accumulated over the last 5000 time steps.

The partial structure factors (PSF) $S_{ij}(k)$, reported below, were calculated by Fourier-transforming the radial distribution functions $g_{ij}(r)$; their values can therefore be considered accurate down to a minimum wavevector $k \simeq 2\pi/L$. However, for each of the simulation runs performed, a systematic comparison was also made in the low-k region between the $S_{ij}(k)$ so obtained and the direct estimate of the density fluctuation correlations average, $\langle \rho_k \rho_{-k} \rangle$; the agreement between the two sets of results was generally satisfactory.

3. Molecular-dynamics results for molten YCl_3

We adopt for this system the representation of [6] in which parameters appearing in (1) are chosen to reproduce the crystalline Y–Cl bond length and the breathing-mode frequency of the $(YCl_6)^{3-}$ octahedron; the existence in molten YCl_3 of such a structural unit has been experimentally established by Raman scattering [12]. The actual values of the potential parameters are reported in the first column ($R_Y = 1.20$ Å) of table 1.

3.1. Structural properties

The neutron structure factor is obtained from the $S_{ij}(k)$, reported in this same section, according to the formula

$$S_n(k) = \sum_{i,j} b_i b_j (c_i c_j)^{1/2} [S_{ij}(k) - \delta_{ij} + (c_i c_j)^{1/2}] \Big/ \left(\sum_i b_i c_i \right)^2$$

where b_i is the coherent neutron-scattering length and c_i the concentration of the ith species, respectively.

A comparison between the MD and experimental $S_n(k)$ is reported in figure 1. As it is possible to see, the agreement of MD with both experiment and HNC [6] is qualitatively good. In particular, a well defined FSDP emerges at $k \simeq 1.25$ Å^{-1}, a wavevector moderately greater than the experimental one; its height, though overestimated by MD, is in better agreement with the experiment than in the HNC case. The positions of other structural features at higher k are also similarly improved with respect to the integral equation results.

Radial distribution functions (reported in figure 2) and partial structure factors obtained compare fairly well with the HNC ones [6], except perhaps for the height of the main peaks in $g_{ij}(r)$, which the HNC underestimates in some cases. Given such an agreement, we can refer the reader to [5, 6] for a full discussion of these structural functions. Here we only note the almost exact sixfold coordination of Cl^- around Y^{3+} obtained, being $n_{YCl} = 5.94$.

Table 1. Parameters used in the simulation of molten MCl_3 systems. Fixed values of some parameters entering the model potential (1) are: $Z_M = +3$, $Z_{Cl} = -1$, $f = 0.05e^2$ Å^{-2}, $R_{Cl} = 1.71$ Å, $\rho_{Cl} = 0.238$ Å, $\rho_M = 0.007$ Å.

	$R_Y = 1.20$ Å	$R_M = 0.82$ Å				$R_M = 1.12$ Å			$R_M = 1.42$ Å
Temperature (K)	1020	700	1020	1020	1020	1020	2100	2100	1020
Number density (Å^{-3})	0.0316	0.0234	0.0117	0.0117	0.0316	0.0316	0.0316	0.0241	0.0316
Particles number	664	384	340	664	340	340	340	340	340
Box length (Å)	27.60	25.41	30.74	38.42	22.07	22.07	22.07	24.15	22.07

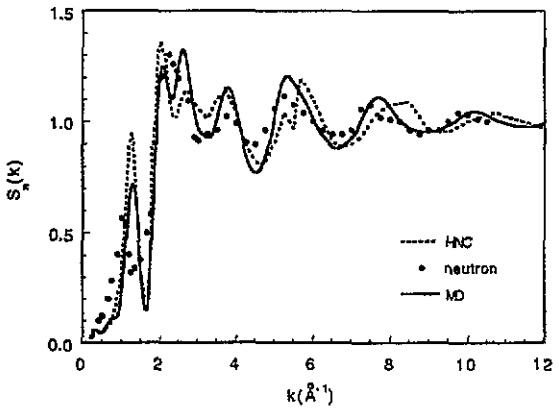

Figure 1. Neutron structure factor in molten YCl_3 at 1020 K: neutron data [4]; HNC [6]; MD (this work).

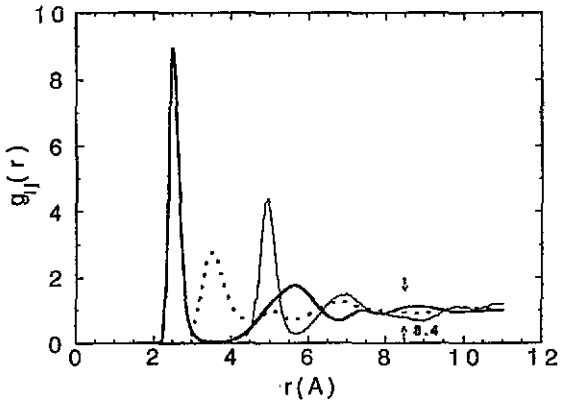

Figure 2. MD radial distribution functions for molten YCl_3 at 1020 K. Thick full curve, Y–Cl; thin full curve, Y–Y; dotted curve, Cl–Cl. Arrows at 8.4 Å indicate the shoulder in $g_{YY}(r)$ discussed in section 3.2.

3.2. Local coordination and MRO

The value of n_{YCl} suggests the formation of $(YCl_6)^{3-}$ octahedra; evidence for such an arrangement is provided both by the ratio $\sim \sqrt{2}$ of the main peak positions in g_{ClCl} and g_{YCl} (see figure 2), as expected in octahedral coordination, and by an analysis of angular distributions (AD).

The latter functions are obtained by calculating for any given ion A the angle defined by the triplet B–Â–B, where B is another ion either of A or B species, usually located within Â's first unlike- or like-neighbour coordination shell. The angular distribution so generated is then averaged over 400 MD configurations. We report in figure 3 the Cl–Ŷ–Cl AD so obtained.

The very well defined peak at 90°, and the broad feature at approximately twice this angle ($\sim$ 170°), are consistent with a slightly distorted $(YCl_6)^{3-}$ octahedral configuration. The Cl–Ĉ–Cl AD, also reported in figure 3, is similarly consistent, since its two peaks at 60° and 90° correspond to the two different manners in which a triplet of chlorines can form an angle on the regular octahedron surface.

In order to investigate how octahedral units are linked to each other, it is useful to look at the Y–Ŷ–Y AD. We compare the results of two different calculations, corresponding to triplets that extend up to the first or to the second like neighbours of the central Ŷ ion, respectively (see $g_{YY}(r)$ in figure 2).

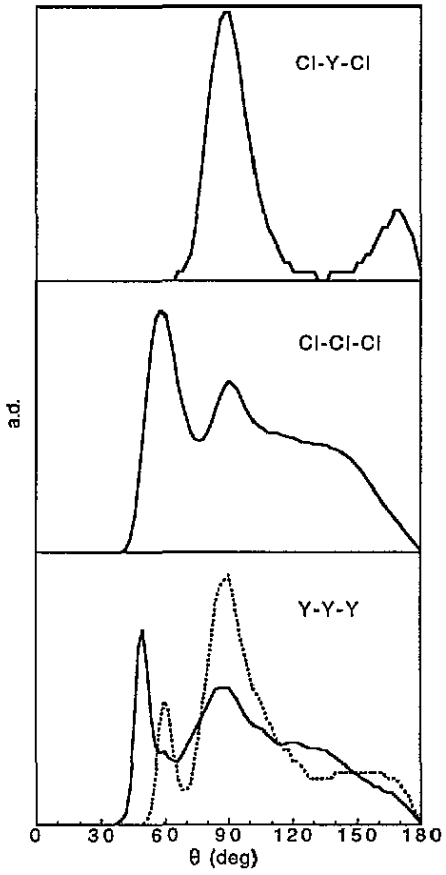

Figure 3. Angular distributions of molten YCl_3 at 1020 K. Y–Ŷ–Y AD: dotted curve, Y ions confined to Ŷ's first like-neighbour shell; full curve, extension to Ŷ's second like-neighbour shell.

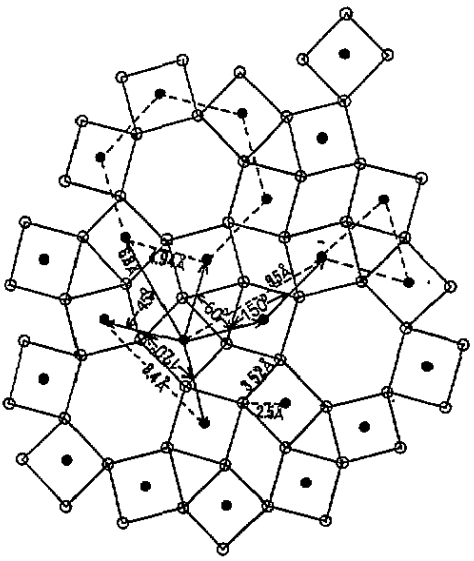

Figure 4. A plane of MD corner-sharing octahedra fulfilling metric and angular relationships discussed in the text. Full circles, Y^{3+} ions; open circles, Cl^- ions. In this view, two chlorines per octahedron rest over and beneath the plane; their projection would overlap the central Y^{3+} ion. Also, an idealized undistorted geometric arrangement is displayed in order to highlight the origin of relevant distances and angles. Note hexagonal and triangular octahedra rings; the last ones are responsible for the 60° feature in Y–Ŷ–Y AD; also note that a great number of 45° Y–Ŷ–Y triplets can be formed by the Ŷ ion with yttriums confined to the second like-neighbour shell (see text).

As can be seen in figure 3, when only first like neighbours are considered, there are two well defined features in this AD, at 60° and 90°, respectively; while when the calculation is extended to the second like-neighbour shell, a third peak appears at ~ 50°; in this second case the 60° feature appears as a shoulder.

Now, the ratio $6.84/4.94 \simeq \sqrt{2}$ of the second to the first peak position in g_{YY} (see figure 2) indicates a square arrangement of Y^{3+} ions, as we shall immediately visualize, and consistent with such a configuration are both the 90° and the 50° angle in Y–$\hat{Y}$–Y AD, the last one roughly corresponding to the 45° angle formed by the diagonal with the edges of the square itself. The feature at 60° in the same AD can instead be associated with triangular arrangements of yttrium ions, as we are also going to show. Finally, we note some other remarkable metric relationships, involving large-r features in g_{YY}: for instance, the ratio $8.4/4.94 \simeq \sqrt{3} = 2\sin 60°$ of the shoulder at 8.4 Å to the first peak position of this RDF, or also the ratio $9.5/4.94 \simeq \sqrt{(2+\sqrt{3})} = 2\sin 75°$ of the third to the first peak position (see figure 2).

The only manner in which all these results can be rationalized seems to assume the existence in the melt of a planar arrangement of *corner-sharing* $(YCl_6)^{3-}$ octahedra, fairly ordered up to g_{YY} third-neighbour shell, as shown in figure 4.

Each octahedron is confined in the 'plane' with four similar units, and with two other out-of-plane octahedra at its top and bottom. The out-of-plane octahedra (obviously not visible in figure 4) may belong to other 'layers'; their angular correlation with octahedra in the 'plane' is rather loose, as can be deduced, for instance, from the broad plateau covering the 110–150° range in the Cl–$\hat{Cl}$–Cl AD (see figure 3).

It is interesting to observe that the proposed arrangement can be generated by using as basic units hexagonal and triangular octahedra rings, as evidenced in figure 4.

Table 2. *Statistics of coordination and links in molten* YCl_3 *and* $AlCl_3$, *at different number densities of particles* ρ and temperatures ($N_M = 85$, $N_{Cl} = 255$).

	YCl_3			$AlCl_3$		
Temperature (K)	1020	2100	2100	1020	1020	700
Number density ($Å^{-3}$)	0.0316	0.0316	0.0241	0.0316	0.0117	0.0234
Y atoms sixfold coordinated	38	36	23			
Bridging chlorines	64	56	27	22	48	58
Edge-sharing octahedra	2.86					
Chains of three corner-linked octahedra	195	157	52			
Al atoms fourfold coordinated				45	60	68
Chains of three corner-linked tetrahedra				16	41	48

3.3. Statistics of links

We now report some results concerning local coordination and linking between $(YCl_6)^{3-}$ local structures.

It appears from table 2 that ~ 38, out of the 85 Y^{3+} ions present in our simulation box, coordinate six chlorines; the octahedra thus formed link to each other mainly through bridging (corner) chlorines, and the number of the latter is relatively high (~ 64). Linking in sequence of three octahedra has also been determined: the number of such chains (~ 195) is also relatively high. As a consequence, only a small percentage of edge-sharing octahedra is present.

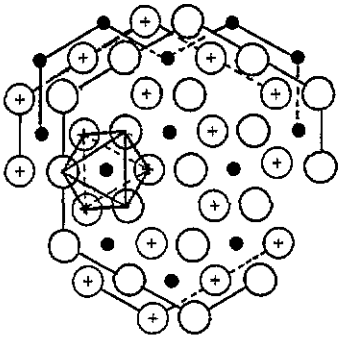

Figure 5. A layer in the idealized $AlCl_3$-type crystal structure in which YCl_3 also crystallizes. Top Cl plane, open circles; bottom Cl plane, crossed circles; interleaved M plane, filled circles. A $(YCl_6)^{3-}$ octahedral unit is also shown.

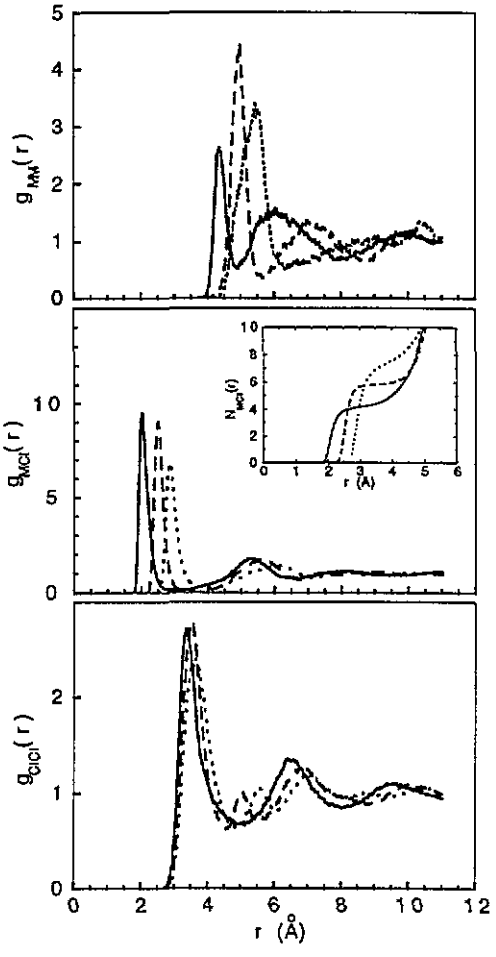

Figure 6. Radial distribution functions at different metal radii. Dotted curve, $R_M = 1.42$ Å; broken curve, $R_M = 1.12$ Å; full curve, $R_M = 0.82$ Å. Inset: n_{MCl} at different metal radii; same symbols as for $g_{ij}(r)$.

These data constitute further evidence that a network of corner-sharing octahedra, characterized by a considerable internal connectivity, is formed in the melt.

Now the structure of crystalline YCl_3 is constituted by layers of *edge-sharing* $(YCl_6)^{3-}$ octahedra, as shown in figure 5, and Saboungi *et al* [4] have deduced the existence of 'a loose disordered network of *edge-sharing* octahedral units in the liquid phase' of YCl_3. Therefore, the MD results indicate an internal ordering of the network that is different from

the crystalline one, and from that hypothesized for the real fused salt. We shall comment on these different network topologies in section 5.

3.4. Density and temperature effects

We now investigate the effect of varying both temperature and density on the structure of molten YCl_3.

We first raise the temperature from 1020 K to 2100 K by keeping the system at the number density appropriate to the lower temperature (see table 1). A slightly different yttrium radius [5,6] ($R_Y = 1.12$ Å, see table 1) and $N = 340$ were used for these simulations. The resulting RDF show little modification with respect to the $T = 1020$ K case.

If we now decrease the density by keeping the temperature fixed at 2100 K, the effect is more remarkable and some of the features associated with local coordination and MRO tend to disappear. In particular, the second peak in $g_{ClCl}(r)$ at ~ 5 Å (see figure 2), corresponding to the distance of two chlorines in any Cl–$\hat{Y}$–Cl diagonal of the octahedron, is almost absent.

The different role played in this context by density and temperature variations, respectively, can also be appreciated from table 2. It appears that the temperature only moderately affects the number of $(YCl_6)^{3-}$ units and of bridging chlorines. Conversely, when the density decreases, the number of octahedra is sensibly reduced and connectivity as well.

We conclude this section by reporting results for the ionic diffusion coefficients. Patterns typical of a fully liquid state are obtained for the mean square displacements, with Cl^- diffusing faster than Y^{3+}, as a result of both mass and charge differences. The ionic self-diffusion coefficients thereby estimated are $D_+ = 0.48 \times 10^{-5}$ cm^2 s^{-1} and $D_- = 0.692 \times 10^{-5}$ cm^2 s^{-1}.

We do not have available any self-diffusion coefficient of molten MCl_3 salts for comparison, but compared to similar data for other types of molten salts the present values could appear rather small: e.g., in NaCl at 1100 K one has $D_- = 6.77 \times 10^{-5}$ cm^2 s^{-1} while in $CdCl_2$ at 883 K $D_- = 2.4 \times 10^{-5}$ cm^2 s^{-1} (see [13]). We see, however, that the anion self-diffusion coefficient tends to decrease when the cation metal valence increases, and specific conductivity data do actually show a similar trend. For instance, at 1146 K one has $\sigma_{NaCl} = 3.800\ \Omega^{-1}$ cm^{-1}, $\sigma_{SrCl_2} = 2.0\ \Omega^{-1}$ cm^{-1} and $\sigma_{YCl_3} = 0.731\ \Omega^{-1}$ cm^{-1}, respectively [13]. Thus, the present estimates of $D_\pm$ though presumably not accurate, could be realistic. We shall further comment on this point in section 5.

4. Size effects

In this section we investigate the effect that the trivalent metal size can have on the formation of a 'network' in molten MCl_3 systems.

We consider in more detail the case of an effective metal radius $R_M = 0.82$ Å, which, in the framework of the assumed model potential (1), corresponds better to the ionic size of Al^{3+} in molten $AlCl_3$ [6]. We shall also report results for $R_M = 1.12$ Å, that is for a situation very similar to the YCl_3 case [5], and for $R_M = 1.42$ Å, an effective radius that could be attributed to La^{3+} in molten $LaCl_3$ [6]. This last correspondence is mentioned here for illustrative purposes; specific MD simulations for lanthanide trichlorides will form the content of a forthcoming paper [14].

4.1. Structural properties versus metal radius

We first consider a case in which the number density of particles is taken equal to that of YCl_3 at 1020 K (see table 1).

Note in figure 6, where RDF are reported, that the number of chlorines coordinated around one metal, n_{MCl}, manifests an evident transition from sixfold to fourfold coordination in passing from $R_M = 1.12$ Å to $R_M = 0.82$ Å. Such a modification is also expressed by the disappearance in $g_{ClCl}(r)$ of the feature at ~ 5 Å associated, as already observed, with chlorines on opposite corners in the octahedron.

Fourfold coordination is obviously consistent with the formation of $(AlCl_4)^-$ tetrahedral units and in fact the Cl–$\hat{M}$–Cl AD peaks at 105°, an angle fairly close to 109°47′ typical of the regular tetrahedral configuration. Similarly the Cl–$\hat{Cl}$–Cl has the expected peak at 60°.

It is now convenient to introduce the density–density structure factor defined as

$$S_{NN}(k) = \sum_{i,j} (c_i c_j)^{1/2} S_{ij}(k).$$

It is well known that $S_{NN}(k)$, like $S_n(k)$, exhibits a FSDP in the presence of MRO [2,3,6,9].

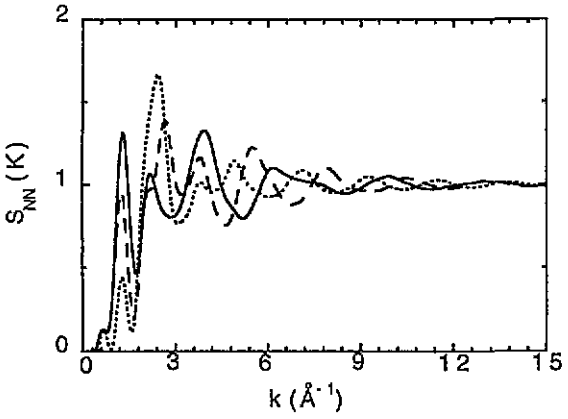

Figure 7. Evolution of the density–density structure factor $S_{NN}(k)$ with the metal radius. Full curve, $R_M = 0.82$ Å; broken curve, $R_M = 1.12$ Å; dotted curve, $R_M = 1.42$ Å.

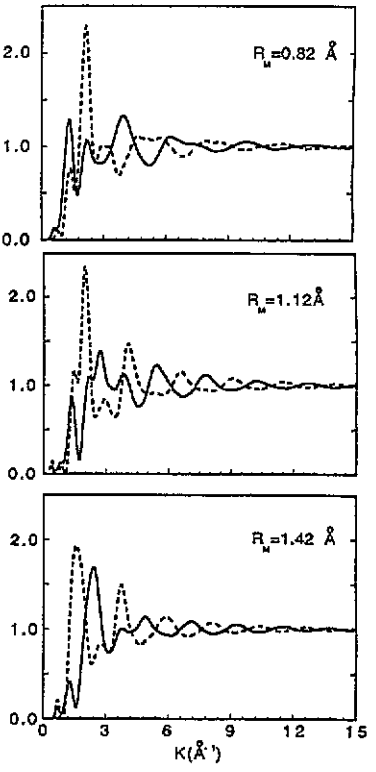

Figure 8. $S_{NN}(k)$ (full curves) and $S_{ZZ}(k)$ (broken curves) at different metal radii.

As can be seen in figure 7, there is a well defined peak at 1.25 Å^{-1} visible in $S_{NN}(k)$ at $R_M = 1.12$ Å, which becomes even larger when $R_M = 0.82$ Å, that is for a smaller metal

radius; the effect is the opposite for the bigger metal case, $R_M = 1.42$ Å. These results confirm the previously reported [6] HNC picture of $S_{NN}(k)$ evolution with metal radius.

4.2. Density and temperature effects; statistics of links

We now consider the density and temperature effects on the structural picture emerging from the previous section. Two different calculations are reported: one at a number density of particles $\rho = 0.0177$ cm^{-3} much lower than that of YCl_3 at 1020 K, and another at $\rho = 0.0234$ cm^{-3} corresponding to *real* $AlCl_3$ at $T = 700$ K [13]. The MD run at 700 K was started from the crystalline configuration shown in figure 5. The melting of such a configuration was monitored through the mean square displacements, which attained liquid-like behaviour.

An estimate of the number of metal ions involved in tetrahedral formation is reported in table 2. This number is rather high in all cases and tends to increase when we lower the density.

Turning to the linkage of $(AlCl_4)^-$ tetrahedra, electroneutrality requires that each tetrahedron shares two chlorines with other similar neighbouring units. This may be realized either with pairs of tetrahedra in an edge-sharing configuration and formation of an Al_2Cl_6 dimer [6], or via corner-linked tetrahedra chains.

As shown in table 2 there is a considerable number of bridging chlorines in $AlCl_3$ at 700 K, and also many three-tetrahedra chains. These results strongly suggest the formation of a network of corner-linked tetrahedra.

As far as the presence of dimers is concerned, we have determined the average number of metal ions, N_{MM}, coordinating only one metal inside their first like-neighbour shell (that is, inside the distance roughly corresponding to the first minimum in $g_{MM}(r)$). In the $AlCl_3$ case ($R_M = 0.82$ Å) at 700 K, ~ 25 out of 85 metal ions coordinate one metal ion. This fact can be interpreted in terms of 'dimer' formation. Moreover, N_{MM} increases from 22 to 32 with decreasing density, while the effect of the metal radius is drastic: at $R_M = 1.12$ Å (YCl_3 case) N_{MM} is almost negligible (~ 2).

We now consider figure 6 and observe that, from g_{MCl} at $R_M = 0.82$ Å, one deduces a first-neighbour M–Cl distance of 2.02 Å. This implies that two metal ions can share one chlorine with a high probability only if their distance does not exceed 4.04 Å. Since the average M–M distance, resulting from the g_{MM} first peak position, is 4.36 Å, such a sharing is practically made possible only by the main peak 'tail' in g_{MCl} (the first minimum of this function falls at 3.12 Å). It follows that the probability for *two* chlorines to be *fully* shared by two neighbouring metal ions, as requested in the edge-sharing tetrahedral configuration, is rather small.

All these MD data seem interpretable in terms of distorted or elongated Al_2Cl_6 'dimer' formation, the corresponding physical arrangement being such that each of the two 'shared' chlorines is actually more tightly bonded to one or the other of the two metals, and a highly coordinated motion of two $(AlCl_4)^-$ tetrahedra is taking place.

The presence of 'elongated' dimers in model liquid $AlCl_3$ has been predicted by Tosi *et al* [6], and the distortion correlated to the unscreened Coulombic repulsion between the highly charged metals. They also found that dimer formation was favoured at low densities, a result that MD confirms, as shown above.

4.3. Charge ordering versus MRO

The MD structure factors turn out to be very similar to the HNC ones in [6], and a discussion of charge ordering in terms of these quantities can be found therein. Here we examine

charge ordering from the point of view of the charge–charge structure factor

$$S_{ZZ}(k) = \sum_{i,j} Z_i Z_j (c_i c_j)^{1/2} S_{ij}(k) \Big/ \sum_i Z_i^2 c_i. \tag{2}$$

The evolution with the metal radius of this structural function is inspected in parallel with that of $S_{NN}(k)$, previously reported. The results are shown in figure 8.

We can see that at $R_M = 0.82$ Å, $S_{ZZ}(k)$ has both a prepeak and a main feature for $k \leqslant 2$ Å^{-1}; the prepeak, noticeably, falls at 1.35 Å^{-1}, very close to the $S_{NN}(k)$ FSDP position. When the metal radius increases, the prepeak evolves into a shoulder, while the main peak shifts to lower k, until at $R_M = 1.42$ Å the shoulder disappears and only one peak is present at $k \sim 1.6$ Å^{-1}.

It appears from the positions and relative heights of the two prepeaks in $S_{NN}(k)$ and $S_{ZZ}(k)$ that, for small metal sizes, charge order coexists, and partially overlaps, with the better defined density medium-range order. For larger metal size, density MRO is almost absent, as proved in the $R_M = 1.42$ Å case, by the relatively low prepeak in $S_{NN}(k)$ at $k = 1.35$ Å^{-1}; conversely, charge ordering persists over distances $\sim 2\pi/(1.6$ Å$^{-1}) = 4$ Å.

Such a situation appears somewhat different from what was found in molten chalcogenides by Vashishta *et al* [8]. In these systems, when the cation-to-anion radius ratio $\alpha > 0.5$, $S_{ZZ}(k)$ does not have any peak or feature for $kd < 4.5$, where d is the sum of the cation and anion radii. Now, as can be deduced from table 1, at $R_M = 0.82$ Å one has $\alpha \sim 0.48$ and $d = 2.53$ Å, so that the prepeak of $S_{ZZ}(k)$ falls at $kd \sim 1.35 \times 2.53 \sim 3.4$. Similarly, it is easy to verify that, at $R_M = 1.12$ Å and $R_M = 1.42$ Å, the first $S_{ZZ}(k)$ feature would fall at $kd \sim 4$ and $kd \sim 5$, respectively. Thus, in our case charge order develops on a distance scale greater than in molten chalcogenides, especially when the ionic species have sensibly different sizes.

We would like to note at this stage that recent MD simulations of $CaSiO_3$ glass [11], based on a rigid-ion potential similar to the one adopted here, while reproducing qualitatively well neutron diffraction data for this compound, showed no evidence of a FSDP at low k in $S_{ZZ}(k)$. However, when the interferential contribution coming from Ca^{2+} and O^{2-} ions were calculated separately in the expression for the total $S_{ZZ}(k)$ (equation (2)), a prepeak was visible in the resulting patterns, positioned practically the same wavevector as the FSDP associated with the density MRO in $S_{NN}(k)$. Therefore, if we focus our attention on the subsystem formed by calcium and oxygen ions, we find charge ordering characteristics similar to those encountered in MCl_3 melts. As discussed in [11], the reciprocal arrangement of Ca^{2+} and O^{2-} species is closely related to their relative size difference, and this confirms the picture emerging before of global charge ordering as intimately related to radius ratio effects.

5. Discussion and conclusions

We have applied the MD simulation technique to a simplified model of molten trivalent metal chlorides. Particles have been assumed to interact via a rigid-ion potential constituted of a short-range repulsive term and long-range Coulombic interaction. The size of the metal ion, entering the potential via an effective radius parameter, has been allowed to vary over a range of values that can realistically correspond to different MCl_3 molten salts.

The case of molten YCl_3 was first studied in detail. It is shown that, in accordance with what has already been found by other authors [5,6], the model is able to predict

the total neutron structure factor of this material in good agreement with the experimental result of Saboungi *et al* [4]. Moreover, after an extensive analysis of coordination numbers, angular distributions and linking properties of the local structural units, it turns out that the layer-like structure of crystalline YCl_3, consisting of planes of edge-sharing $(YCl_6)^{3-}$ octahedra, persists locally in the liquid phase with formation of a roughly planar structure of corner-sharing octadhedra. Such a 'planarity' approximately extends up to the yttrium third like-neighbour shell.

Now, in interpreting their neutron diffraction data, Saboungi *et al* came to the conclusion that a loose network of edge-sharing octahedra should be present in molten YCl_3. Our results actually indicate the formation of a network characterized by a moderate internal connectivity; however, we find little evidence of edge-sharing octahedra configurations. We conjecture that this last result may be due to the neglect of polarization effects in our model; actually, the corner-sharing octahedra configuration is such that the highly charged Y^{3+} ions can stay at the maximum distance compatible with the sharing of one chlorine; obviously, screening associated with polarization would moderate such a repulsion and presumably favour a closer arrangement of metals like that of the edge-sharing configuration.

The absence of polarization terms in potential (1) has the consequence of emphasizing the role of Coulombic forces, and this may be one reason for the rather low self-diffusion coefficients obtained in section 3. Another, and possibly more important, cause may be the fact that in our model we are ignoring internal molecular vibrations; the presence of these would make it much easier for the molecules to get past each other, thus increasing the diffusion constant, especially when diffusion is highly hindered anyway. Obviously, a definite assessment of this point could come only from a comparison of D_+ and D_- with experimental data. More generally, it would be worth further testing the reliability of the model through MD simulations for other lanthanide trichlorides for which structural data are available [6]. We are currently planning such an investigation [14].

As far as the effect of metal size on the structural properties and medium-range order is concerned, the MD simulations confirm the previously found transition of chlorines from octahedral to tetrahedral coordination when passing from the bigger Y^{3+} in molten YCl_3 to the smaller Al^{3+} in molten $AlCl_3$. Our calculations show that small metal size favours the formation of a highly connected network of corner-sharing tetrahedra responsible for the presence of MRO in this size regime.

Mixed into such tetrahedra chains are distorted 'dimers' constituted by two $(AlCl_4)^-$ tetrahedra; their presence, predicted earlier in model liquid $AlCl_3$ by Tosi *et al* [6], is quantified here through a detailed investigation of the MD configurations. Interest in such formations mainly stems from the existence of Al_2Cl_6 dimers in real molten $AlCl_3$; it appears, in fact, that the same model potential (1) is qualitatively capable of describing, in terms of metal radius variation, the markedly different structure of two melts, YCl_3 and $AlCl_3$ respectively, which are known to crystallize in the same structure shown in figure 5. In other words, the model results suggest strong cation size effects in the different melting mechanisms of the two compounds [4, 6].

Since we have adopted a representation of our molten salts that totally disregards covalence and polarization effects, our analysis and conclusions cannot be considered as more than indicative. However, other studies [2, 3, 6, 9] have shown that the details of the short-range structure rather than the global scenario of the medium-range order are improved when the interparticle model potential is so refined. Moreover, our results are fully consistent with a broad analysis of structural correlations in metal halide melts, recently performed by Tosi *et al* [15].

The qualitative agreement with experimental data achieved here, and similar

performances previously obtained for glasses where the same rigid-ion model has been assumed [11], point to a major role of geometric versus Coulombic ordering effects in determining the medium-range structure of a wide class of mainly ionic materials.

Acknowledgments

Useful contacts with Professor M Tosi are acknowledged.

References

[1] Philips J C 1981 *J. Non-Cryst. Solids* **43** 37
[2] Vashishta P, Kalia R K and Ebbsjö I 1989 *Phys. Rev.* B **39** 6034 and references therein
[3] Iyetomi H, Vashishta P and Kalia R K 1991 *Phys. Rev.* B **43** 1726
[4] Saboungi M L, Price D L, Scamehorn C and Tosi M P 1991 *Europhys. Lett.* **15** 283
[5] Pastore G, Akdeniz Z and Tosi M P 1991 *J. Phys.: Condens. Matter* **3** 8297
[6] Tatlipinar H, Akdeniz Z, Pastore G and Tosi M P 1992 *J. Phys.: Condens. Matter* **4** 8933
[7] Erbolukbas A, Akdeniz Z and Tosi M P 1992 *Nuovo Cimento* D **14** 87
[8] Iyetomi H and Vashishta P 1993 *Phys. Rev.* B **47** 3063
[9] Vashishta P, Kalia R K, Rino J P and Ebbsjö I 1990 *Phys. Rev.* B **41** 12 197
Rino J P, Ebbsjö I, Kalia R K, Nakano A and Vashishta P 1993 *Phys. Rev.* B **47** 3053
[10] Wilson M and Madden P A 1993 *J. Phys.: Condens. Matter* **5** 6833
[11] Abramo M C, Caccamo C and Pizzimenti G 1992 *Phys. Lett.* **166A** 65; 1992 *J. Chem. Phys.* **12** 9083
[12] Papatheodorou G N 1977 *J. Chem. Phys.* **66** 2893
[13] Janz G J 1967 *Molten Salts Handbook* (New York: Academic)
[14] Abramo M C and Caccamo C to be submitted
[15] Tosi M P, Price D L and Saboungi M L 1993 *Ann. Rev. Phys. Chem.* **44** 173